Pernice, F., De Carvalho, N., & Hallett, S. (2017). Prediction of delamination migration at a 0°/θ ply interface in composite tape laminates. In *31st Annual Technical Conference of the American Society for Composites 2016: Proceedings of a meeting held 19-22 September 2016, Williamsburg, Virginia, USA. Held with the Annual ASTM Committee D30 Meeting* (Vol. 1, pp. 352-367). [1704] http://dpi-proceedings.com/index.php/asc31/article/view/3094

Peer reviewed version

COVER SHEET

Paper Number: **1704**

Title: **Prediction of delamination migration at a 0°/θ ply interface in composite tape laminates**

Authors: M. Francesca Pernice
Nelson V. De Carvalho
Stephen R. Hallett

ABSTRACT

Delamination in composite laminates can migrate through the thickness, from one interface to another. The "Delamination Migration" test method allows a detailed observation of migration, and the evaluation of the parameters affecting it. Delamination migration tests conducted on specimens containing a $0°/\theta$ interface demonstrated that migration is governed by the sign of the component of interlaminar shear stress perpendicular to the θ fiber direction, τ_{23}. At a $0°/\theta$ interface, when the shear stress sign is favorable for migration, delamination tends to propagate along the θ fiber direction, before migrating through the θ-oriented ply. The conditions at the $0°/\theta$ interface, which determine either delamination growth along the θ fiber direction or migration, were evaluated using the Virtual Crack Closure Technique (VCCT). The strain energy release rates in the direction of the fibers, G_f, and perpendicular to the fibers, G_m, were calculated, along with the total strain energy release rate, G_T. The components G_f and G_m were then used with the shear stress sign, to account for the effect of both parameters on delamination growth and migration. Correlation with experimental results for 0°/60° delamination migration specimens showed that if the sign of τ_{23} is favorable for migration but G_f/G_T is greater than G_m/G_T, delamination tends to propagate along the θ fiber direction and migration will not occur. Delamination can migrate only if G_f/G_T is less than G_m/G_T. This method improves the prediction of migration in the delamination migration specimen, compared to the analysis using the shear stress sign only.

M. Francesca Pernice, Advanced Composites Centre for Innovation and Science (ACCIS), University of Bristol, Queen's Building, University Walk, BS8 1TR, Bristol, U. K.

Nelson V. De Carvalho, National Institute of Aerospace, resident at: Durability, Damage Tolerance and Reliability Branch, NASA Langley Research Center, Hampton, VA 23681-2199, U.S.A.

Stephen R. Hallett, Advanced Composites Centre for Innovation and Science (ACCIS), University of Bristol, Queen's Building, University Walk, BS8 1TR, Bristol, U. K.

INTRODUCTION

Delamination in composite laminates often propagates at interfaces between plies with dissimilar fiber orientation and can migrate through the thickness of the laminate from one ply interface to another, by means of an intralaminar crack. Delamination migration is commonly observed in laminates subject to low-velocity impact damage [1, 2] or at structural singularities such as skin/stiffener joints [3] and open holes [4]. Under both static and fatigue loading conditions, delamination migration can cause the propagation of damage through the thickness of a laminate, potentially leading to the global failure of a composite structure. A number of experimental studies have focused on delamination migration, in order to gain a better understanding of this damage mechanism [5-8].

Delamination migration is governed by the sign of the interlaminar shear stress at the delamination front [5, 7]. Delamination growth and migration result from the coalescence of microcracks at the delamination front. The microcracks are perpendicular to the resolved tensile stress produced by shearing of adjacent plies, and angled at 45º with respect to the interface [9, 10]. For a given delamination growth direction, the microcracks are oriented towards one of the plies at the interface, depending on the shear stress sign (Figure 1). The resulting delamination tends to propagate close to or through the thickness of that ply. If the fiber direction in the ply is aligned with the delamination growth direction (as in Figure 1a), then the intralaminar fracture is prevented, since propagation of a crack through the ply thickness would break the fibers. Delamination thus stays at the interface and propagates along the fiber direction, as demonstrated experimentally in [6, 7, 11]. Conversely, if the fiber direction in the ply towards which delamination is driven is angled with respect to the direction of shear, then the fibers do not prevent propagation of delamination through the ply (Figure 1b), and migration becomes possible [5, 7].

This process was demonstrated experimentally at a 0º/90º interface using the Delamination Migration test in [7]. The delamination migration test is designed on the assumption that delamination propagation and migration are governed by the sign of the interlaminar shear stress, as in [5]. The resulting experiment allows the isolation of one single migration event at a 0°/90° interface and the observation of the mechanism by which delamination turns out (or "kinks out") of the interface and migrates to the next interface.

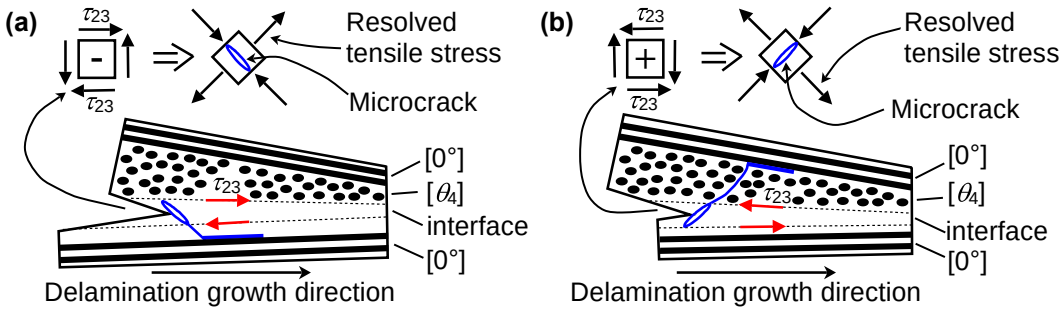

Figure 1. Effect of shear stress sign at the delamination front on the orientation of microcracks and the subsequent delamination growth and migration.

In [8], the delamination migration test was used to observe migration at a $0^o/\theta$ interface (with $\theta = 60^o, 75^o$). It was found that at a $0^o/\theta$ interface, the component of shear stress governing delamination migration is the component perpendicular to the θ fiber direction, τ_{23}. When the sign of τ_{23} at a $0^o/\theta$ interface drives delamination towards the upper θ ply, delamination propagates close to the θ ply and migration is favored. Delamination tended to propagate along the θ fiber direction in the upper bounding ply, or delamination kinked out of the interface into the θ ply and the kinked cracks propagated along the θ fiber direction, before migration was completed. The study concluded that the favorable shear stress sign is a condition necessary for delamination migration at a $0^o/\theta$ ply interface, but it is not sufficient [8].

The work presented here is based on the experimental results reported in [8] and investigates the conditions at the delamination front at the $0^o/\theta$ interface which determine whether delamination propagates at the interface along the θ fiber direction or migrates through the thickness of the θ-oriented ply. The Virtual Crack Closure Technique (VCCT) [12, 13] was employed to calculate the strain energy release rates at the delamination front in the $0^o/60°$ specimens. Similar to the τ_{23} component of shear stress used in [8], strain energy release rates were then evaluated to determine propensity for delamination to propagate at the interface or migrate, in terms of the components of strain energy release rate aligned with the θ fiber coordinate system. The propensity for delamination to either propagate at the initial interface along the θ fiber direction or migrate was evaluated by a parameter which combines the effect of the fiber-aligned strain energy release rates and the effect of the sign of the interlaminar shear stress, τ_{23}.

SUMMARY OF EXPERIMENTAL RESULTS

This work uses experimental results obtained in [8], in which delamination migration tests were performed on specimens containing a $0°/\theta$ interface. The Delamination Migration test [7] is briefly described here, followed by a summary of the main results presented in [8], before the analytical method used here is explained.

The Delamination Migration Test

The Delamination Migration test [7] is designed to isolate and investigate in detail delamination migration. A schematic representation of the delamination migration specimen in the test fixture is displayed in Figure 2. The test employs a beam-type specimen containing a 12.7-μm-thick polytetrafluoroethylene (PTFE) film insert ("T") at one end in a $0^o/T/90^o_4/0^o$ sequence (ordered from the bottom to the top surface of the specimen), to create an artificial delamination, a_0, Figure 2. The test configuration allows for a reversal in the interlaminar shear stress sign during the test, starting from a "negative" sign, which drives delamination towards the lower 0^o ply at the $0^o/90^o$ interface (as in Figure 1a), to a "positive" sign, which drives delamination towards the upper 90^o ply at the $0^o/90^o$ interface (as in Figure 1b). This shear stress sign reversal, together with the specific $0^o/T/90^o_4/0^o$ ply stack in the specimen, results in delamination growth from the PTFE insert front at the beginning of the test (negative shear stress sign), where the lower 0^o fibers prevent migration through the

ply. After the shear stress sign reverses and becomes positive, the upper 90º fibers cannot confine crack growth to the interface, and delamination may now kink out of the original interface and migrate to the next 90º/0º interface, through the 90^{o}_{4} ply stack [7].

The location of the load-application point, referred to as "load offset", L in Figure 2, can be changed along the length of the specimen. Changing the load offset affects the loading conditions at the delamination front in the delamination migration specimen and, consequently, the location of kinking and migration, and demonstrates the dependence of migration on the shear stress sign at the delamination front. Full details of the delamination migration test can be found in [7].

In [7], it was proposed that, after the shear stress sign reverses in the specimen, delamination will kink out of the interface only when it is energetically favorable, according to the energy criterion (He and Hutchinson criterion for isotropic materials [14]):

$$\frac{G_k}{G_{IC}} > \frac{G}{G_C} \tag{1}$$

where G_k and G are maximum strain energy release rates for the kinked crack and for the interface crack (0º/90º delamination), respectively. Here, G_{IC} is the mode I critical strain energy release rate of the material into which the kinked crack propagates (in this case the 90º ply) and G_C is the critical strain energy release rate of the interface. The energy condition in eq. (1) could predict whether delamination continues to propagate along the initial ply interface in the specimen or kinks out of the interface and propagates through the upper ply stack, given that the shear stress sign is favorable.

The original specimens tested in [7] employed a 0°/90° interface, to obtain a uniform delamination migration event across the specimen width, which provides benchmarking data for advanced modeling techniques [15]. In [8], the delamination migration test method was employed to investigate delamination migration at a 0°/θ ply interface. The main results are summarized in the next section.

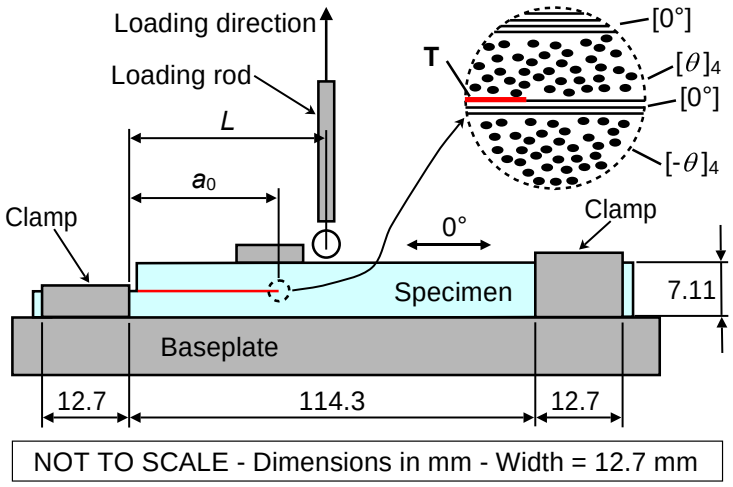

Figure 2. Schematic of the delamination migration test set-up (adapted from [8]).

Delamination Migration at a 0°/60° Ply Interface

In [8], delamination migration tests were performed on specimens containing a 0°/θ interface. The specimen stacking sequence was designed in order to contain the 0º/T/θ_4/0º ply stack required for the test and minimize coupling effects. The 56-ply stacking sequence for the 0º/θ specimens was (from the bottom to the top surface of the specimen): [θ/ 0º/ θ_3/ -θ_4/ -α/ -θ/ -α/ 90º/ -α/ α/ 90º/ α/ θ/ α/ θ_4/-θ_4/ 0º/ T/ θ_4/ 0º/ -θ_4/ -α/ -θ/ -α/ 90º/ -α/ α/ 90º/ α/ θ/ α/ θ_4/ 0º/ -θ_4], where θ = {60º, 75º}, α = (90º - θ) and "T" indicates the location of the PTFE film insert. Specimen dimensions are shown in Figure 2. The initial artificial delamination length, a_0, was 53 mm. Specimens were made from IM7/8552 carbon fiber epoxy tape. Tests were run at different values of load offset, L. Details of the experimental tests and evaluation of the shear stress sign can be found in [8]. Results obtained for load offset $L = a_0$ in specimens containing a 0°/60° ply interface are briefly summarized here.

Figure 3 shows an X-ray Computed Tomography (CT scan) image of the upper 60° delamination surface of a specimen after testing, together with two longitudinal sections close to the specimen edges. The damage sequence was obtained by incremental tests, performed by partially loading the specimen and then inspecting it by X-ray CT scan before continuing the test. Specimen edges were denoted as "front" and "rear" edge, as shown in Figure 3. Results showed that delamination kinked out of the 0º/60° interface at several locations inside the specimen (Points 1 and 2 in Figure 3), although these kinking events were not visible on the specimen edges. At these points, delamination propagated close to the upper 60° ply at the interface and kinked through it, without completing migration, as displayed by the detail of the arrested kinked cracks in Sec. B-B in Figure 3. Under further loading of the specimen, the 0°/60° delamination or the kinked cracks propagate along the 60° fiber direction, towards the rear edge of the specimen.

Using linear elastic finite element analysis, a correlation was found between the location inside the specimen where kinking started (Points 1 and 2 in Figure 3) and the location of reversal of the sign of the shear stress component, τ_{23}. Analyses at increasing delamination lengths showed that the shear stress component, τ_{23}, varies across the width of the specimen at a 0°/60° interface and, consequently, the shear stress sign reversal is not uniform across the specimen width. Figure 4 shows the variation of τ_{23} across the width of the specimen, from the front edge (y = 0) to the rear edge (y = 12.7 mm), at different delamination lengths, Δc (values are normalized by absolute value of the τ_{23} obtained in the center of the specimen, $|\tau_{23,c}|$, as shown in the figure). At the beginning of the test, the shear stress sign is negative across the entire width of the specimen (driving delamination towards the lower 0° ply), in agreement with the experimental observation that delamination propagated at the original 0°/60° interface, starting from the PTFE insert front. The observed location of initiation of kinking corresponded to the region across the specimen width and the delamination length at which the shear stress sign reverses first. In particular, the initiation of kinking (Points 1 and 2 in Figure 3) took place at a distance ΔW_k from the front edge of the specimen ranging between 7 and 11 mm and a delamination length Δc_k between 4 and 11 mm, in all the specimens tested [8]. Finite element analyses showed that the shear stress sign reverses (and becomes positive and, therefore, favorable for migration) at a delamination length of 5 mm and a location across the

specimen width between 6.35 and 10 mm from the front edge [8]. The correlation between experimental results and shear stress sign demonstrates that delamination can only kink out of the original interface if the shear stress sign is favorable (positive).

Test results showed that, under further loading of the specimen, additional kinking events took place inside the specimen (Points 3 to 6 in Figure 3) and they were all contained in the rear side region of the specimen (between the center and the rear edge), which agrees with the location inside the specimen where shear stress sign reverses first (Figure 4). Eventually, one of the kinked cracks propagated through the thickness of the $60_4°$ ply stack and completed migration (Point 8 in Figure 3). Conversely, in the front side region of the specimen (between the front edge and the center) delamination stayed at the original 0°/60° interface until migration was completed (Point 9 in Figure 3), because in this region the shear stress sign reverses at a delamination length greater than in the rear side region of the specimen (Figure 4). Since in the front side region, the shear stress sign is negative, delamination is driven towards the lower ply at the interface and propagates along the 0° fiber direction.

Delamination migration at a 0°/θ interface [8] differed from the 0°/90° interface case [7], because, after the shear stress sign reverses and becomes favorable for migration, the delamination at the 0°/θ interface or the kinked cracks propagate along the θ fiber direction, in some cases without completing migration. This propagation along the θ fiber direction raises the question about the conditions which determine whether a crack propagates along the θ fiber direction or migrates through the θ oriented ply stack. These conditions are investigated in this work.

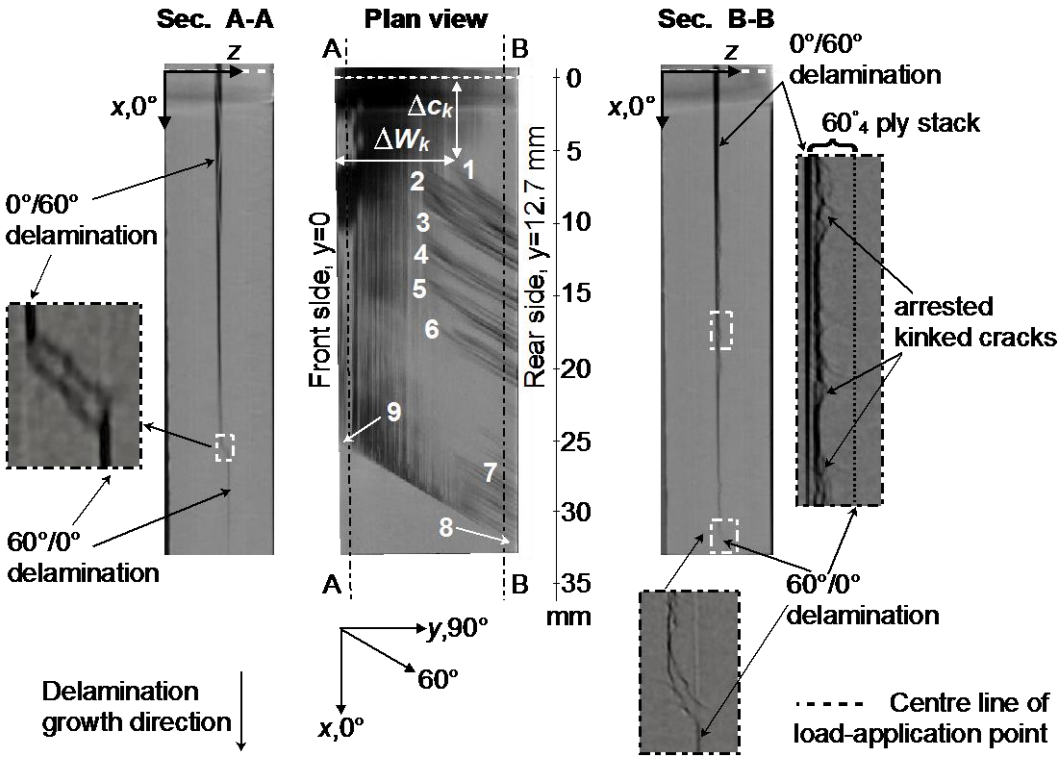

Figure 3. X-ray CT scan image of the upper 60° delamination surface in a specimen containing a 0°/60° interface and longitudinal sections near the specimen edges (adapted from [8]).

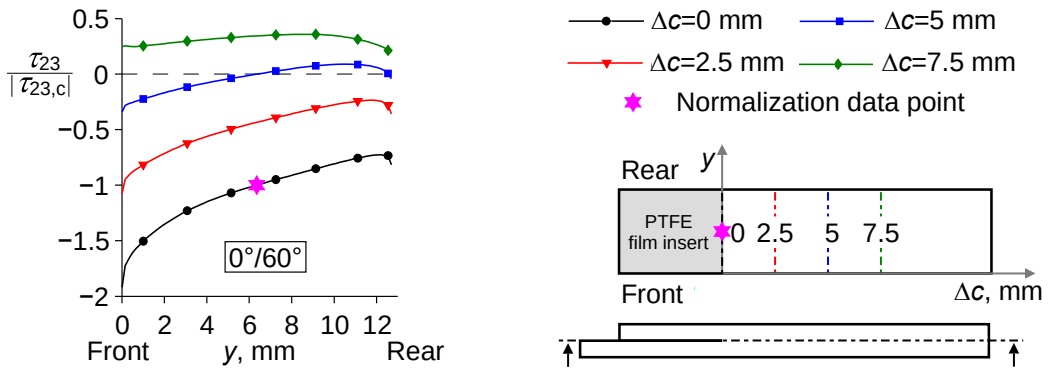

Figure 4. Shear stress distribution across the specimen width at increasing delamination length, Δc, at a 0°/60° interface (adapted from [8]).

FIBER-ALIGNED VCCT

The propagation of damage along the θ fiber direction in the 0°/θ specimens suggests that before the criterion in eq. (1) can be evaluated, a condition must be met at the 0°/θ interface, so that the delamination does not propagate along the θ fiber direction, but tends to grow in a direction transverse to the fiber and will eventually migrate through the ply. The analyses performed in this work evaluate this condition in terms of the strain energy release rate at the 0°/θ interface, rather than within the ply through which the delamination may migrate. The Virtual Crack Closure Technique [12, 13] was employed to evaluate the strain energy release rates at the delamination front at a 0°/60° interface and correlate them to the observed propagation of delamination or kinked cracks along the 60° fiber direction.

Similar to the interlaminar shear stress component, τ_{23} [8], strain energy release rate components in directions parallel and perpendicular to the θ fibers were calculated. These components of strain energy release rate, taken with respect to the fiber orientations, are said to describe delamination propagation and migration at an interface between plies with dissimilar fiber orientation better than the traditional mode II and mode III components [16, 17]. Here, the fiber-aligned strain energy release rates were combined with the information derived from the evaluation of the interlaminar shear stress sign, in order to obtain a parameter that can describe propensity for delamination to propagate along the θ fibers or migrate.

Numerical Model for 3D VCCT Analyses of 0°/60° Specimens

Three-dimensional finite element analyses of a delamination migration specimen containing a 0°/60° ply interface and loaded at load offset $L = a_0$ were conducted in Abaqus/Standard, version 6.12 [18]. The one-step Virtual Crack Closure Technique, which requires a single analysis step at each different delamination length, was performed in a post-processing step. A three-dimensional model was employed, in order to obtain the distribution of strain energy release rates along the delamination front. The model used corresponds to the model previously used in [8] to evaluate the shear stress sign at the delamination front and is depicted in Figure 5.

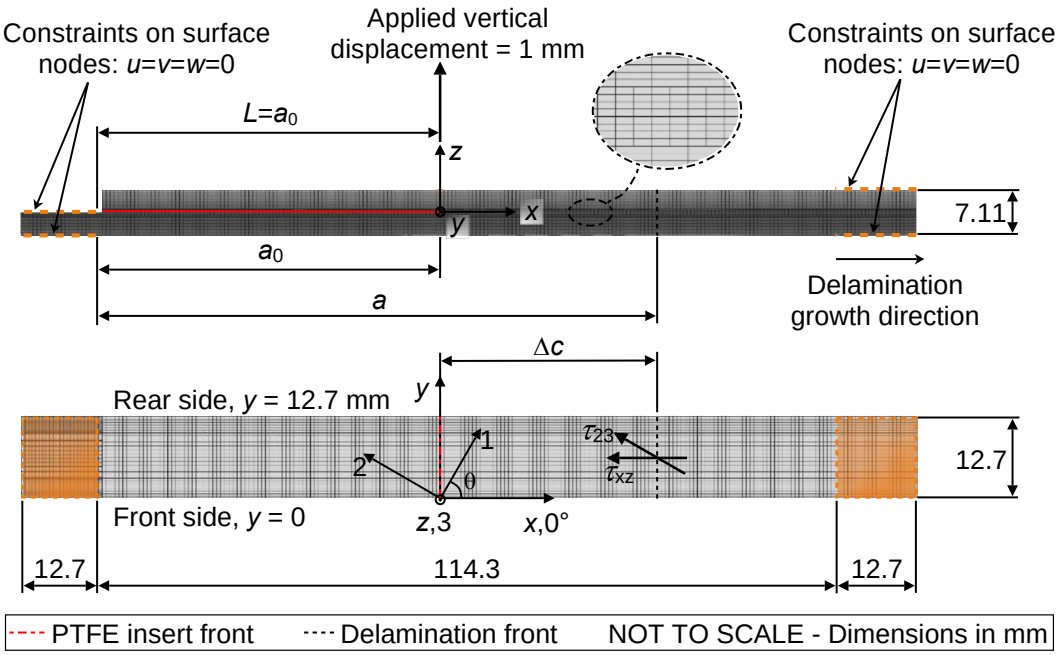

Figure 5. Finite element model of the 0°/60° delamination migration specimen [8].

TABLE I. Material properties for IM7/8552 [19].

E_{11}	E_{22}	E_{33}	ν_{12}	ν_{13}	ν_{23}	G_{12}	G_{13}	G_{23}
GPa	GPa	GPa				GPa	GPa	GPa
161.0	11.38	11.38	0.32	0.32	0.436	5.17	5.17	3.98

The specimen model had a total length of 139.7 mm and width of 12.7 mm. One layer of eight-node brick elements (Abaqus type C3D8) was used for each ply, assuming a ply thickness of 0.127 mm. Element size was kept constant along the specimen length but it was refined along the specimen width, to account for possible edge effects. The orthotropic material properties of IM7/8552 carbon/epoxy tape reported in Table I [19] were assigned in the model. The clamped boundary conditions on the specimen in the delamination migration test fixture were idealized by clamping a 12.7-mm-long portion of the specimen on both ends.

Load was applied as a fixed vertical displacement equal to 1 mm. A straight delamination front was assumed, in agreement with the shape of the delamination front observed during incremental tests in [8]. Increasing delamination lengths were modeled, in order to evaluate the effect of strain energy release rate on delamination growth and migration as delamination length increases during the test. Analyses were performed at a delamination length equal to the initial artificial delamination, a_0, and then at fixed delamination lengths increased by Δc = {2.5, 5, 7.5, 10, 12.5, 15} mm (Figure 5). The initial artificial delamination was modeled by coincident nodes in the region of the specimen containing the PTFE film insert. The intact portion of the specimen was modeled by applying multipoint constraints to the nodes at the 0°/60° interface, in the region ahead of the delamination front. The multipoint constraints were successively removed to increase the delamination length in a series of analyses, as Δc increases.

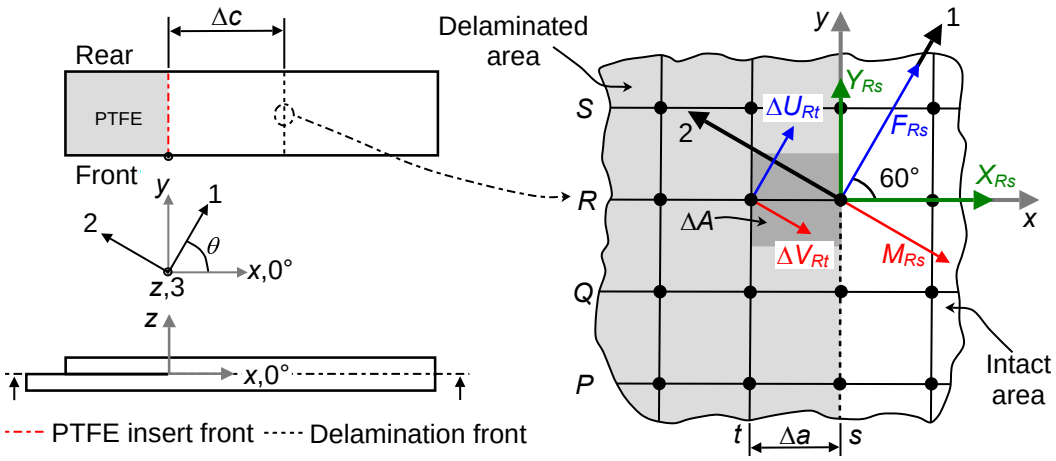

Figure 6. Forces and relative displacements in the local coordinate system aligned with the 60° fibers (1, 2, 3) for calculation of local strain energy release rate components.

Local Components of Strain Energy Release Rate

Forces and relative displacements for the calculation of strain energy release rates were obtained from the model. For each delamination length modeled, the nodal force at each node at the crack tip along the delamination front was obtained by summing the contributions from the four elements with a common node belonging to the upper arm of the specimen, above the delamination plane (two elements in case of nodes at the edges of the specimen). Displacements at nodes behind the delamination front, at a distance Δa from the crack tip (equal to the element length), were obtained from the model, for each delamination length. Relative displacements were calculated as the difference between the displacement in the node at the upper face and the displacement in the corresponding node at the lower face at the delamination. Forces and relative displacements obtained from the model are in the coordinate system of the specimen, (x, y, z), where x is the 0° fiber direction along the specimen length (Figure 5).

A local coordinate system (1, 2, 3) was defined for each node at the delamination front, with 1 being the direction of the fibers in the upper 60° ply at the interface, 2 the direction perpendicular to the 60° fibers and 3 the through the thickness direction (coincident with z). The global (x, y, z), in grey, and local (1, 2, 3), in black, coordinate systems are shown in Figure 6. In the figure, node position along the delamination front is indicated by upper case letters (such as Q, R), while lines of nodes parallel to the delamination front are identified by lower case letters (such as s, t) [13]. The forces at a node Rs at the delamination front obtained from the model (X_{Rs} in direction x and Y_{Rs} in direction y, Figure 6) were rotated by an angle $\theta = 60°$ to obtain the forces in the local coordinate system (1, 2, 3), F_{Rs} (blue arrow) and M_{Rs} (red arrow). In the same way, the relative displacements obtained from the model in the global coordinate system, Δu_{Rt} and Δv_{Rt} in node Rt behind the delamination front, were rotated to obtain the relative displacements in the local coordinate system of the fibers, ΔU_{Rt} (blue arrow) and ΔV_{Rt} (red arrow):

$$\begin{pmatrix} F_{Rs} \\ M_{Rs} \end{pmatrix} = \begin{bmatrix} \cos\theta & \sin\theta \\ -\sin\theta & \cos\theta \end{bmatrix} \begin{pmatrix} X_{Rs} \\ Y_{Rs} \end{pmatrix}, \qquad \begin{pmatrix} \Delta U_{Rt} \\ \Delta V_{Rt} \end{pmatrix} = \begin{bmatrix} \cos\theta & \sin\theta \\ -\sin\theta & \cos\theta \end{bmatrix} \begin{pmatrix} \Delta u_{Rt} \\ \Delta v_{Rt} \end{pmatrix} \tag{2}$$

where θ is the fiber angle in the ply where strain energy release rates need to be calculated.

The local forces and relative displacements obtained by eqs. (2) were used to calculate the fiber-aligned component of strain energy release rate. Strain energy release rates in the fiber direction, G_f, and perpendicular to the fiber direction (or "matrix" direction in a ply), G_m, were calculated. The component G_f along the fiber direction is related to delamination growth along the fibers, while the component G_m is thought to be related to delamination migration, similar to the shear stress component, τ_{23}. The mode I component, G_I, in the direction of the laminate thickness was also calculated, to obtain the total strain energy release rate $G_T = G_I + G_f + G_m$. The local component of strain energy release rate along the fiber direction, G_f, in a node *Rs* at the delamination front is given by the component of force in fiber direction, F_{Rs}, in the same node *Rs*, and the component of relative displacement in fiber direction, ΔU_{Rt}, in node *Rt* behind the delamination front (as shown in Figure 6). Similarly, the local component of strain energy release rate in the direction perpendicular to the fibers, G_m, in a node *Rs* at the delamination front is given by the component of force in the direction perpendicular to the fibers in node *Rs*, M_{Rs}, and the component of relative displacement in the direction perpendicular to the fibers, ΔV_{Rt}. The local strain energy release rates were divided by the total strain energy release rate, G_T, in order to normalize the strain energy release rate, and allow comparison between strain energy release rates at different delamination lengths. Using the notation in Figure 6, and considering the force Z_{Rs} and relative displacement Δw_{Rt} in the opening direction, the following quantities were calculated:

$$\frac{G_f}{G_T} = \frac{F_{Rs}\Delta U_{Rt}}{Z_{Rs}\Delta w_{Rt} + F_{Rs}\Delta U_{Rt} + M_{Rs}\Delta V_{Rt}} \tag{3}$$

$$\frac{G_m}{G_T} = \frac{M_{Rs}\Delta V_{Rt}}{Z_{Rs}\Delta w_{Rt} + F_{Rs}\Delta U_{Rt} + M_{Rs}\Delta V_{Rt}} \tag{4}$$

$$\frac{G_I}{G_T} = \frac{Z_{Rs}\Delta w_{Rt}}{Z_{Rs}\Delta w_{Rt} + F_{Rs}\Delta U_{Rt} + M_{Rs}\Delta V_{Rt}} \tag{5}$$

Absolute values of forces and relative displacements were used for calculations of the strain energy release rates. For each delamination length, Δc, strain energy release rate components G_f and G_m were calculated with reference to the ply towards which delamination is driven by the shear stress sign at that delamination length (either 0° or θ). A local coordinate system aligned to the fibers in the selected ply was defined, and the local components of strain energy release rate, G_f and G_m, were calculated. At the beginning of the test, for delamination lengths, Δc, such that $\tau_{23} < 0$, strain energy release rates were evaluated with reference to the lower 0° bounding ply at the interface. The 0° fiber direction coincides with the *x*-axis in the finite element model of the delamination migration specimen and, consequently G_f is

equal to the mode II component. However, strain energy release rate components aligned to the 0° fibers and perpendicular to the 0° fibers were calculated using eqs. (3) and (4), respectively, assuming a fiber angle $\theta = 0°$ in eqs. (2), for consistency with the strain energy release rates calculated with reference to the upper ply at the interface. As delamination grows, the shear stress sign at the delamination front reverses, and delamination is driven towards the upper ply at the interface. Therefore, for delamination length, Δc, at which $\tau_{23} > 0$, strain energy release rates were evaluated with reference to the upper bounding ply at the interface. Local strain energy release rates were calculated for either the upper or the lower ply at the interface (depending on the shear stress sign) in order to evaluate the effect of the local components G_f and G_m on delamination growth and migration throughout the test, from the onset at the PTFE insert front to migration.

Results obtained by the VCCT analyses (G/G_T) were combined with the shear stress sign to account for its effect on kinking and migration. A parameter, k, was defined as follows:

$$k_i = \frac{G_i}{G_T} * \text{sign}(\tau_{23}) = \begin{cases} -\frac{G_i}{G_T}, & \text{if } \tau_{23} < 0 \\ +\frac{G_i}{G_T}, & \text{if } \tau_{23} \geq 0 \end{cases}, \qquad i = (f, m) \qquad (6)$$

where the index i denotes the direction parallel or perpendicular to the fibers in the ply towards which delamination is driven. The parameters k_f and k_m account for the effect of shear stress sign and strain energy release rates on delamination and are used in the following section to evaluate propensity for delamination to propagate along the fiber direction or to kink and migrate.

RESULTS AND DISCUSSION

The propensity for delamination to kink out of the interface is evaluated by comparing values of k_f, in the direction parallel to the fibers, and k_m, in the direction perpendicular to the fibers, for each ply at the interface. Plots of k_i concisely show the effect of local components of strain energy release rate and the effect of sign of shear stress τ_{23} at the interface on delamination growth and migration. Results are plotted along the delamination front, as a function of the distance across the specimen width, y (see Figure 5), for each delamination length, Δc. The distance y is measured from the front side of the specimen, $y = 0$, to the rear side of the specimen, $y = 12.7$ mm. Plots of k_f and k_m are shown and discussed for the lower 0° bounding ply at the interface if $\tau_{23} < 0$, and for the upper 60° bounding ply if $\tau_{23} > 0$.

At a 0°/60° ply interface, at delamination lengths $\Delta c = \{0, 2.5\}$ mm, the shear stress sign is negative across the entire width of the specimen (Figure 4). Conversely, at delamination length $\Delta c = 5$ mm, the shear stress sign varies across the specimen width and it is negative only in the front side region of the specimen (Figure 4). In these negative shear stress sign locations at the interface, strain energy release rates were calculated in a local coordinate system aligned to the 0° fibers in the lower ply at the interface, using eqs. (3-5), and assuming a rotation angle equal to 0° for forces and relative displacements in eqs. (2). Figure 7 shows k_f and k_m across the specimen width

for the lower 0° ply at a 0°/60° interface, for delamination lengths Δc = {2.5, 5} mm. At the onset from the PTFE insert front (Δc = 0 mm), results were similar to the case Δc = 2.5 mm, and are omitted for brevity. Local directions of the strain energy release rate components G_f and G_m in the 0° ply are illustrated in the sketch in the figure. For delamination length Δc = 2.5 mm, the shear stress sign is negative across the entire width of the specimen (Figure 4). Figure 7a shows that at Δc = 2.5 mm, the value of the strain energy release rate component along the 0° fiber direction (given by the magnitude of $k_{f,0^\circ}$) is greater than the component perpendicular to the fibers:

$$\left|k_{f,0^\circ}\right| > \left|k_{m,0^\circ}\right| \Leftrightarrow \frac{G_{f,0^\circ}}{G_T} > \frac{G_{m,0^\circ}}{G_T} \tag{7}$$

indicating that delamination growth along the 0° fiber direction is favored. This result is in agreement with the experimental observation that delamination onset from the PTFE insert front propagates at the 0°/60° interface, along the 0° fibers [8].

For delamination length Δc = 5 mm, in the front side region of the specimen (at a distance from the front edge $0 \leq y \leq 6.35$ mm), the shear stress sign is negative (Figure 4) and the strain energy release rate component perpendicular to the 0° fibers direction (given by the magnitude of $k_{m,0^\circ}$) is greater than the component along the 0° fiber direction (Figure 7b):

$$\left|k_{m,0^\circ}\right| > \left|k_{f,0^\circ}\right| \Leftrightarrow \frac{G_{m,0^\circ}}{G_T} > \frac{G_{f,0^\circ}}{G_T} \ . \tag{8}$$

This result indicates that propagation of delamination along the 0° fiber direction is no longer favored, although the shear stress sign drives delamination towards the 0° ply. For delamination length Δc = 5 mm, the shear stress sign is also negative on the extreme rear edge of the specimen as shown in Figure 4. Figure 7b shows that the strain energy release rate component along the 0° fiber direction at the rear edge is greater than the component perpendicular to the fiber (eq. (7)), indicating that delamination propagation along the 0° fiber direction is favored.

At a delamination length Δc = 5 mm, the shear stress sign changes from negative to positive at slightly less than halfway from the front to the rear edge of the specimen. For greater delamination lengths, it becomes positive across the entire width of the specimen (Figure 4). In these cases, strain energy release rates were calculated in a local coordinate system aligned to the 60° fiber direction in the upper ply at the interface. Forces and relative displacements were calculated using eqs. (2) and assuming a rotation angle equal to 60°. The local directions of G_f and G_m in the 60° ply are illustrated in the sketch in Figure 8. In the figure, $k_{f,60^\circ}$ and $k_{m,60^\circ}$ are plotted across the specimen width, at delamination lengths such that the shear stress sign is positive.

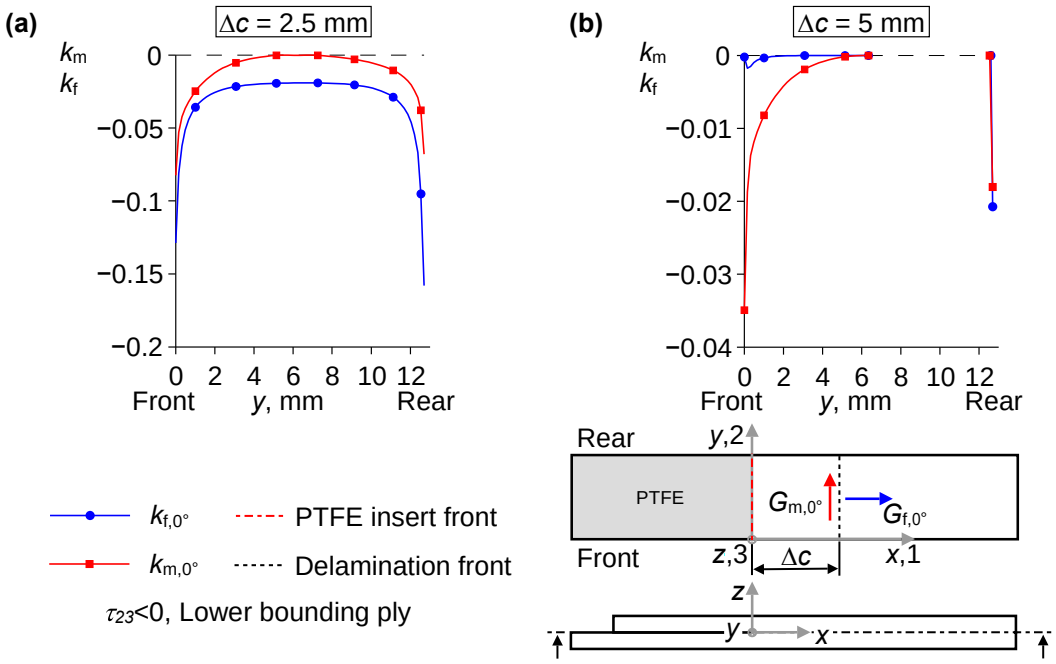

Figure 7. Comparison between $k_{f,0^\circ}$ and $k_{m,0^\circ}$ across the specimen width in the lower 0° ply at a 0°/60° interface at different delamination lengths.

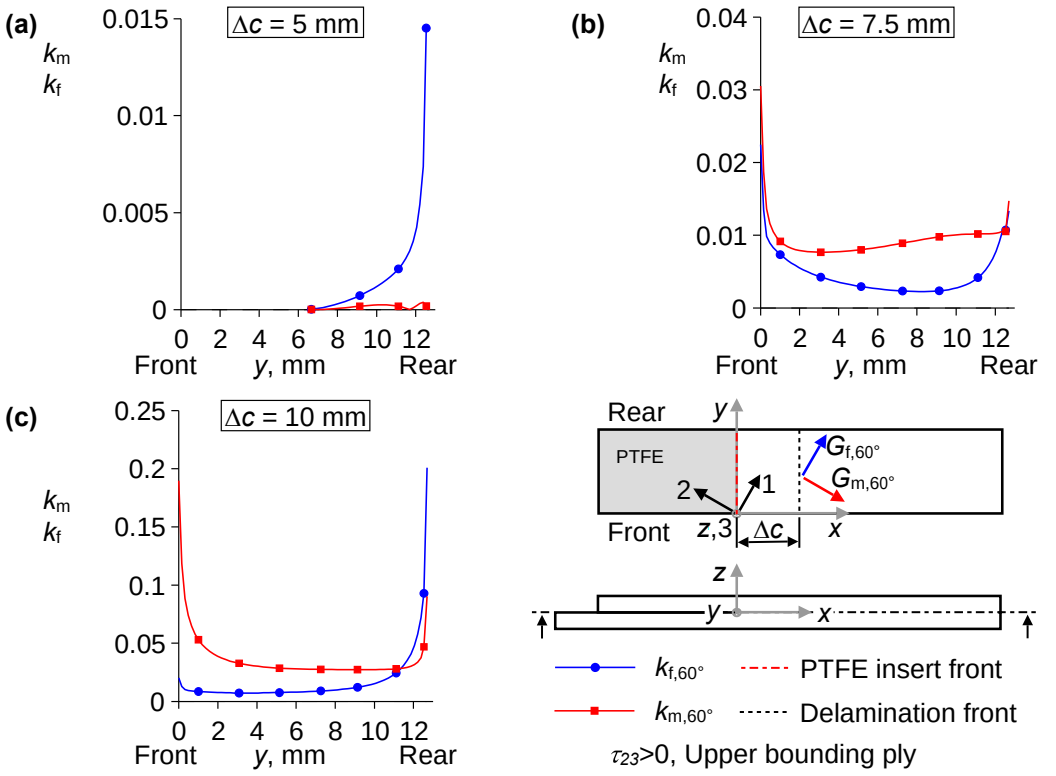

Figure 8. Comparison between $k_{f,60^\circ}$ and $k_{m,60^\circ}$ across the specimen width in the upper 60° ply at a 0°/60° interface at different delamination lengths.

At delamination length Δc = 5 mm and at a distance from the front edge of the specimen $6.35 \leq y \leq 12.7$ mm (rear side region of the specimen), the shear stress is positive and tends to drive delamination towards the upper 60° ply at the interface (Figure 4). This condition has been found to be necessary for migration [8]. However, Figure 8a shows that the strain energy release rate component along the 60° fiber direction (given by the magnitude of $k_{f,60°}$) is greater than the component perpendicular to the fibers:

$$\left|k_{f,60°}\right| > \left|k_{m,60°}\right| \Leftrightarrow \frac{G_{f,60°}}{G_T} > \frac{G_{m,60°}}{G_T} \tag{9}$$

which indicates that it is energetically more favorable for delamination to propagate along the 60° fiber direction in the upper ply at the interface, rather than kink into the upper ply stack.

As delamination length increases, for Δc = 7.5 mm and greater, the strain energy release rate component along the 60° fiber direction (given by the magnitude of $k_{f,60°}$) becomes less than the component perpendicular to the fibers (given by the magnitude of $k_{m,60°}$) (Figure 8b):

$$\left|k_{f,60°}\right| < \left|k_{m,60°}\right| \Leftrightarrow \frac{G_{f,60°}}{G_T} < \frac{G_{m,60°}}{G_T} \ . \tag{10}$$

In this condition, delamination growth along the 60° fiber direction is not energetically favorable anymore, but delamination tends to propagate in the direction perpendicular to the fibers and can kink into the upper ply stack, because of the greater value of G_m.

Figure 8c shows that, as delamination continues to grow, in a region close to the rear edge of the specimens the strain energy release rate component along the 60° fiber direction becomes greater than the component perpendicular to the fibers, eq. (9). This might explain why the kinked cracks were observed to turn back to the original interface on the rear edge, without completing migration, although the propagation of cracks through the specimen thickness is governed by conditions inside the upper ply stack and not at the interface.

In summary, if the shear stress sign drives delamination towards the upper 60° ply at the 0°/60° interface, and G_f is greater that G_m, delamination tends to propagate along the 60° fiber direction and migration will not occur. The analysis of delamination propagation and migration using both the sign of the shear stress component, τ_{23}, and the local components of strain energy release rate, G_f and G_m, in the fiber coordinate system, provides a better prediction of delamination growth and migration at a 0°/60° ply interface, compared to the evaluation of the shear stress sign only. In Table II, the predictions of kinking obtained from the shear stress sign and from the fiber-aligned strain energy release rates are compared to the measured location of initiation of kinking in specimens tested in [8]. The fiber-aligned strain energy release rates improve prediction, since they allow the distinction between conditions at the interface which are favorable for kinking, and conditions favorable for delamination growth along the fiber direction at a 0°/60° interface.

TABLE II. MEASURED [8] AND CALCULATED LOCATIONS OF KINKING INITIATION

	Delamination length, Δc, mm
Measured location of kinking initiation [8]	4 to 10 (mean value: 7)
Calculated location of shear stress sign reversal [8]	5
Calculated location of favorable strain energy release rate	7.5

The traditional mode II and mode III strain energy release rates would not provide a good description of the delamination behavior at a 0°/60° interface because they cannot describe delamination propagation along the 60° fiber direction, close to the upper 60° ply. For the 0°/60 interface studied, the local strain energy release rate components aligned to the fibers and perpendicular to the fibers provide further information, compared to the traditional mode II and mode III, allowing a prediction of whether delamination propagation along the 60° fibers or kinking is favorable, given that the shear stress drives delamination towards the upper ply at the 0°/60° interface.

CONCLUDING REMARKS

Delamination propagation and migration at a 0°/60° ply interface was investigated using the strain energy release rate components aligned to the fiber direction and perpendicular to the fiber direction at the delamination front in a delamination migration specimen. The information obtained was combined with the sign of the interlaminar shear stress, τ_{23}, which is known to govern delamination migration, to obtain plots of a parameter, k_i, which accounts for both shear stress sign and strain energy release rate. Analyses results were correlated to delamination migration tests on 0°/60° specimens [8].

Correlation between the numerical and the experimental results shows that if the shear stress sign at the delamination front is positive (favorable for migration), and the strain energy release rate along the 60° fiber direction, G_f, is greater than the component perpendicular to the fibers, G_m, delamination migration is prevented, and delamination will be confined at the 0°/60° interface and propagate along the 60° fiber direction. Migration will only occur if the strain energy release rate along the 60° fiber direction, G_f, is less than the component perpendicular to the fibers, G_m.

These results improve the prediction of initiation of kinking in the 0°/60° delamination migration specimens, because they account for propagation of damage along the 60° fiber direction. The traditional mode II and mode III components of strain energy release rate would not allow a complete description of delamination propagation and migration at an interface between plies with dissimilar fiber orientation. Therefore, this study demonstrates the suitability of the use of fiber-aligned strain energy release rate at those interfaces.

ACKNOWLEDGEMENTS

This work was supported by the Engineering and Physical Sciences Research Council (EPSRC), UK, through the EPSRC Centre for Doctoral Training in Advanced Composites for Innovation and Science (grant number EP/G036772/1). The work was additionally supported by the National Aeronautics and Space Administration

(NASA), Langley Research Center, USA, under Research Cooperative Agreement No. NNL09AA00A awarded to the National Institute of Aerospace. Special thanks to Dr. James Ratcliffe of NASA for the invaluable technical discussions.

REFERENCES

1. Cantwell, W.J., and J. Morton. 1991. "The impact resistance of composite materials – A review," *Composites*, 22(5):347-362.
2. Hull, D., and Y.B. Shi. 1993. "Damage mechanism characterization in composite damage tolerance investigations," *Compos. Struct.*, 23:99-120.
3. Krueger, R., M.K. Cvitkovich, T.K. O'Brien and P.J. Minguet. 2000. "Testing and analysis of composite skin/stringer debonding under multi-axial loading," *J. Compos. Mater.*, 34(15):1263-1300.
4. Hallett, S.R., B.G. Green, W.G. Jiang and M.R. Wisnom. 2009. "An experimental and numerical investigation into the damage mechanisms in notched composites," *Compos. Part A*, 40:613-624.
5. Greenhalgh, E.S., C. Rogers, and P. Robinson. 2009. "Fractographic observations on delamination growth and the subsequent migration through the laminate," *Compos. Sci. Technol.*, 69:2345-2351.
6. Canturri, C., E.S. Greenhalgh, S.T. Pinho and J. Ankersen. 2013. "Delamination growth directionality and the subsequent migration process – The key to damage tolerant design," *Compos. Part A*, 54:79-87.
7. Ratcliffe, J.G., M.W. Czabaj, and T.K. O'Brien. August 2013. "A test for characterizing delamination migration in carbon/epoxy tape laminates," National Aeronautics and Space Administration Technical Memorandum NASA/TM-2013-218028.
8. Pernice M.F., N.V. De Carvalho, J.G. Ratcliffe, and S.R. Hallett. 2015. "Experimental study on delamination migration in composite laminates," *Compos. Part A*, 73:20-34.
9. O'Brien, T.K. 1998. "Composite interlaminar shear fracture toughness, G_{IIC}: shear measurement or shear myth?," in *Composite Materials: Fatigue and Fracture (Seventh Volume) ASTM-STP 1330*, R. B. Bucinell, ed. Philadelphia: American Society for Testing and Materials, pp. 3-18.
10. Purslow, D. 1986. "Matrix fractography of fiber-reinforced epoxy composites," *Composites*, 17(4): 189-303.
11. Ratcliffe, J.G., and N.V. De Carvalho. July 2014. "Investigating delamination migration in composite tape laminates," National Aeronautics and Space Administration Technical Memorandum NASA/TM-2014-218289.
12. Rybicki, E.F., and M.F. Kanninen. 1977. "A finite element calculation of stress intensity factors by a modified crack closure integral," *Eng. Fract. Mech.*, 9(4): 931-938.
13. Krueger, R. 2004. "Virtual crack closure technique: History, approach, and applications," *Appl. Mech. Rev.*, 57(2):109-143.
14. He, M.Y., and J.W. Hutchinson. 1989. "Kinking of a crack out of an interface," *J. Appl. Mech.*, 56:270-278.
15. De Carvalho, N.V., B.Y. Chen, S.T. Pinho, J.G. Ratcliffe, P.M. Baiz and T.E. Tay. 2015. "Modeling delamination migration in cross-ply tape laminates," *Compos. Part A*, 71:192-203.
16. Suemasu, H., and Y. Tanikado. 2015. "Damage growth behavior and interlaminar fracture resistance of CFRP laminates under shear fracture mode," *Adv. Compos. Mater*, 24(5):451-466.
17. Canturri, C., E.S. Greenhalgh and S.T. Pinho. 2014. "The relationship between mixed-mode II/III delamination and delamination migration in composite laminates," *Compos. Sci. Technol.*, 105:102-109.
18. ABAQUS/Standard Version 6.12 User's Manual, 2012.
19. O'Brien, T.K., and R. Krueger. 2003. "Analysis of flexure tests for transverse tensile strength characterization of unidirectional composite," *J. Compos. Tech. Res.*, 25:50-68.